Scanning Microscopy Vol. 12, No. 1, 1998 (Pages 149-160) 0891-7035/98$5.00+.25
Scanning Microscopy International, Chicago (AMF O'Hare), IL 60666 USA

DISLOCATION LUMINESCENCE IN CADMIUM TELLURIDE

H.S. Leipner*, J. Schreiber, H. Uniewski and S. Hildebrandt

Fachbereich Physik, Martin-Luther-Universität Halle-Wittenberg

(Received for publication February 3, 1996 and in revised form November 4, 1996)

Abstract

Cathodoluminescence scanning electron microscopy provides a detailed analysis of the dislocation rosette patterns around micro-indentations in cadmium telluride. The activation of a variety of slip systems causes different contrast features, connected to α, β, and screw dislocations. Cross-slip plays an important role for the distribution of defects around indentations. A luminescence line at about 1.48 eV occurring in certain parts of the dislocation rosette is probably related to vacancies. The mechanisms responsible for the generation of vacancies are the interaction of dislocations belonging to different slip systems and the dragging of jogs. The vacancies, which are located near or on dislocations generated by room-temperature indentation, anneal after a thermal treatment at 500 K.

Key Words: Cathodoluminescence, cathodoluminescence contrast, recombination, deformation, defects, dislocations, point defects, semiconductors, compound semiconductors, cadmium telluride.

*Address for correspondence:
H.S. Leipner
Fachbereich Physik
Friedemann-Bach-Platz 6
Martin-Luther-Universität
D-06108 Halle, Germany
Telephone number: (49) 345-5525453
FAX number: (49) 345-5527563
E-mail: leipner@physik.uni-halle.de

Introduction

Cadmium telluride is a II-VI compound semiconductor of sphalerite structure. Recently, bulk CdTe crystals have become important for optoelectronic applications. It is a suitable substrate material for cadmium mercury telluride, which is being used in infrared detectors. The preparation of single crystals is rather difficult, since CdTe can easily be deformed at room temperature [12] and remains ductile down to 77 K. The density of grown-in dislocations in CdTe is higher than in gallium arsenide and lies typically in the order of magnitude of 10^5 to 10^6 cm^{-2}. As there is a non-negligible concentration of residual impurities after crystal growth, the interaction between dislocations and point defects is an important factor for the electrical properties of bulk crystals. The relation of the electronic structure of CdTe and dislocations has been a subject of several studies in recent years (see, e.g., the review of Osip'yan *et al*. [21]). There are features that are unique for II-VI compounds, such as the large photoplastic effect (i.e., the change of the flow stress by illumination) [11] or deformation-induced changes of optical properties. The deformation-induced luminescence in ZnS (triboluminescence) has been attributed to a charge transfer to impurity centers by moving dislocations [4]. Dislocation-related luminescence has been studied in CdS and has been related to the radiative recombination of bound excitons [28].

The crystallographic structure of dislocations in cadmium telluride is very similar to that of gallium arsenide. The glide motion is determined by the Peierls mechanism and the slip systems are of a $<1\bar{1}0>\{111\}$ type. Moving dislocations are generally dissociated into partial dislocations [20, 27]. In cathodoluminescence (CL) and electron-beam induced current imaging at room temperature, dislocations in CdTe appear as dark spots or lines, i.e., they act as centers of nonradiative recombination [22, 24].

Gelsdorf and Schröter [9] showed that the introduction of dislocations in CdTe produced a deep level of 0.7 eV below the conduction band. This level was not attributed to dislocation core states but to a point defect cloud near dislocations. However, the nature of these defects remained unclear. Further investigations by deep level transient spectroscopy (DLTS) [16, 29] supported the hypothesis of a point-defect atmosphere.

The aim of the study presented here was to investigate the correlation between the structure and the electrical activity of dislocations introduced by room-temperature deformation of CdTe. A convenient way to introduce dislocations at low temperatures is micro-indentation. The generation of electrically active defects around micro-indentations on different surfaces of CdTe was studied in detail by cathodoluminescence scanning electron microscopy (CL-SEM). The active slip systems in respect to the emission of α, β, or screw dislocations are analyzed. Peculiar CL contrast features in the deformed region are discussed. Dislocation-related non-radiative and radiative recombination can be distinguished and is related to the influence of an atmosphere of vacancies around dislocations.

Experimental

The investigations were carried out with nominally undoped cadmium telluride single crystals grown by the Bridgman technique. The carrier concentration was in the range of $p = (1 - 5) \times 10^{15}$ cm^{-3}. The grown-in dislocations were mostly arranged in a cell-like structure and their density was $(1 - 9) \times 10^{5}$ cm^{-2}. The (001), $(\overline{1}11)$Te, and (111)Cd surfaces were chemo-mechanically polished with a solution of bromine in methanol. The polarities of ±(111) surfaces were determined according to Brown *et al*. [6]. After etching in a solution of HF-HNO_3-CH_3COOH (1:1:1 vol.%), the $(\overline{1}11)$Te plane appeared bright and shiny, while the (111)Cd plane appeared dull. (110) surfaces were obtained by cleaving the single crystal. The $[1\overline{1}0]$ and [110] directions on a (001) surface were distinguished by etching the crystal in the E.Ag-1 solution (10 ml HNO_3 + 20 ml H_2O + 4 g $K_2Cr_2O_7$ + 1 mg $AgNO_3$), which produces etch pits elongated in a [110] direction [17]. The micro-deformation was carried out at room temperature by indenting the surface with a Vickers diamond pyramid (with an angle of 136° between the pyramid faces). The load was in the range of 0.05 to 1 N and the dwell time about 30 seconds. The defect distribution was analyzed by cathodoluminescence scanning electron microscopy with sample temperatures in the range of 5 to 300 K. For the investigations, a TESLA BS 300 scanning electron microscope ((TESLA, Brno, Czech Republic) equipped with a Oxford Mono-CL system and cryostage ((Oxford Instruments Ltd., Oxford, UK) was used. The experiments were carried out with an electron beam voltage and current of 15 to 25 kV and 1 to 10 nA, respectively. The luminescence signal was detected with a S20 photo-multiplier. The available resolution of panchromatic CL imaging was about 0.2 μm. CL spectra were recorded with a grating monochromator (1200 lines/mm) at different positions of the deformed region. The distribution of radiative centers was registered by spectral CL imaging.

Additional information about defects in the deformed region of the indentation was obtained by transmission electron microscopy (TEM) investigations with a JEOL 1000 high voltage microscope (JEOL, Tokyo, Japan).

Results and Discussion

Slip pattern on ±(111) surfaces

The basic features of the distribution of dislocations near the surface are shown in Figure 1. Generally, the slip processes can be divided into two sets: (i) dislocation movement with Burgers vectors parallel to the surface ("rosette glide") and (ii) dislocation glide with Burgers vectors inclined to the surface ("tetrahedral glide"). The rosette glide is characterized by some 100 μm long branches of dislocations in $\pm[1\overline{1}0]$, $\pm[01\overline{1}]$, $\pm[\overline{1}01]$ directions, respectively. The tetrahedral glide is represented by the triangular pattern of dislocations near the indentation center.

The slip patterns around Vickers hardness indentations on ±(111) surfaces were extensively studied for GaAs by Hirsch *et al*. [14]. First results for (111) CdTe were presented by Riviére *et al*. [22]. The Hirsch model, based on elastic stress field calculations of the indentation zone, is fully applicable to the determination of slip systems and the sense of slip close to the indenter, i.e., to the tetrahedral glide in CdTe. For this set, dislocation glide proceeds on tetrahedral {111} planes. According to the diatomic structure of CdTe, two types of {111} planes have to be considered: Cd-terminated {111} planes and Te-terminated $\{\overline{1}11\}$ planes. Correspondingly, two types of tetrahedra occur, one with the apex internal (IAT), another one with its apex external (EAT) in reference to the sample surface. The polarity of 60° dislocations generated at the indentation depends on the type of the glide plane [25] (Table 1). According to the conception of Sumino and Shimizu [25], α dislocations, with the extra half plane inside, are formed on the {111}Cd tetrahedron. Similarly, β dislocations are on $\{\overline{1}11\}$Te planes, with the extra half plane inside the tetrahedron. It should be noted that in contrast to the original considerations [25], the dislocations are here supposed to be in the glide set.

Basically, slip occurs on both the IAT and the EAT, leading to the generation of α and β dislocations. However, the slip patterns are not symmetrical for the Cd and Te surfaces. It can be deduced from the different dislocation configurations of the tetrahedral glide for (111)Cd and $(\overline{1}11)$Te surfaces (Fig. 1) that glide occurs preferentially only on one type of tetrahedron for a given sample orientation. Regarding the elastic strain field calculations of Hirsch *et al*. [14], glide on the IAT dominates the formation of the triangular slip line pattern in (111)Cd-oriented samples, whereas the extension of the slip pattern for a $(\overline{1}11)$Te surface is due to preferential glide on the EAT. The activation of one type of tetrahedron, which is external for a $(\overline{1}11)$Te surface and internal for (111)Cd, is immediately connected with the generation of α dislocations near the indentation (see Table 1).

Detailed TEM investigations of III-V semiconductors

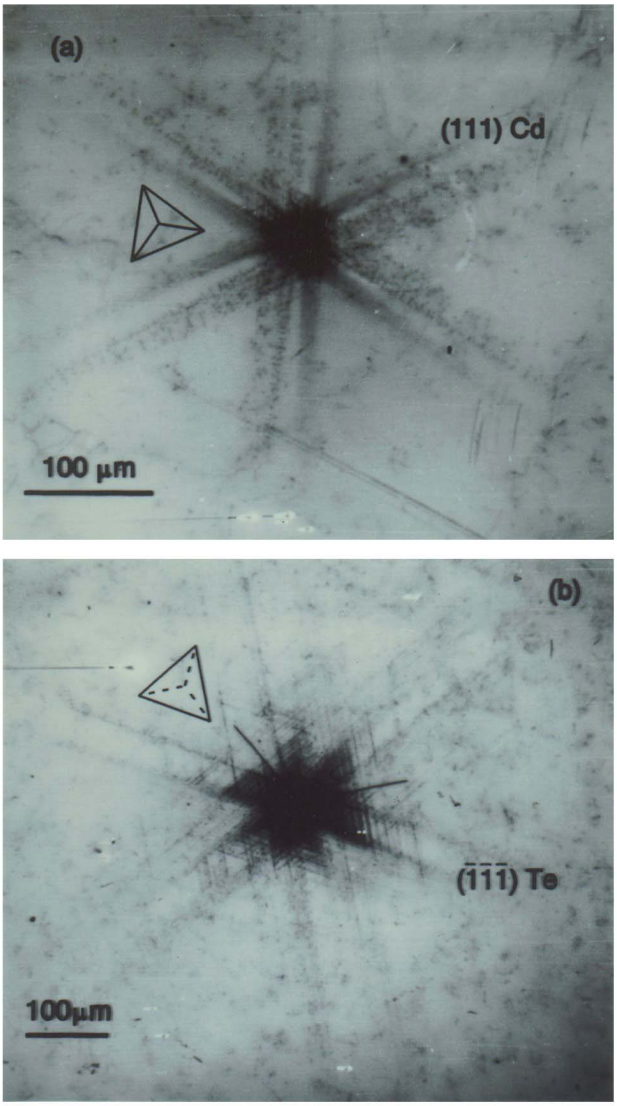

Figure 1. Dislocation distributions near indentations (**a**) on the (111)Cd and (**b**) on the Te surface of CdTe. Panchromatic cathodoluminescence images taken at room temperature (20 kV electron beam). The indentation load was 1 N.

have been carried out in order to study the structure of dislocations generated during micro-deformation [15, 18, 19]. It has been found that slip proceeds preferentially through the motion of dislocation half loops. They include two parallel screws of opposite sense, connected by segments which can be regarded as two 60°α dislocations (or two β dislocations, respectively). In III-V semiconductors, the whole dislocation structure around indentations could be explained by the dynamics of such "hexagonal" loops. The origin of stacking faults (or microtwins) [18, 19] and the formation of locks [26]

Table 1. Tetrahedra of different polarity and related 60° glide-set dislocations [25].

Sample Surface	Internal Apex Tetrahedron	External Apex Tetrahedron
(111)Cd	Cd tetrahedron Te(g)	Te tetrahedron Cd(g)
$(\bar{1}\bar{1}\bar{1})$Te	Te tetrahedron Cd(g)	Cd tetrahedron Te(g)

Note: Te(g) and Cd(g) correspond to α and β dislocations with their extra half plans internal to the tetrahedron concerned. The glide set g is supposed.

could also be described within this model. Despite the much higher dislocation density in CdTe in the region deformed by indentation, the basic structure of hexagonal loops is confirmed by TEM investigations. As it was found in III-V compounds, the dislocation sources are localized at the surface formed by the Vickers pyramid. A scheme of the dislocation loop formation is shown in Figure 2 for the IAT. Dislocation loops on the EAT are formed in a similar way.

A complete understanding of the slip pattern of tetrahedral glide can only be reached by considering recovery processes. The residual stress field near the indentation is supposed to be high enough that dynamic recovery takes place. The recovery is driven by cross-slip of the screw parts of the hexagonal loops. The high stress brought about by the indentation supports the cross-slip, which is impeded by the dissociation of the screw in the primary slip plane. The activation energy of the cross-slip, *U*, depends on the stacking fault energy γ [8],

$$U = -\frac{E_0^2}{\gamma} \ln\frac{\tau}{\tau_0} \qquad (1)$$

(E_0 and τ_0 are constants, τ is the resolved shear stress.) A higher cross-slip activity could be expected in CdTe, since it has a lower stacking fault energy (11 meV per atom [10]), compared to elemental and III-V semiconductors.

The cross-slip mechanisms for both the IAT and the EAT are schematically shown in Figures 3a and 3b. A screw dislocation with the Burgers vector **b** = **AD** on the ACD plane cross-slips on a plane parallel to ABD. The cross-slip is driven by the high stress near the indenter. Furthermore, Lomer-Cottrell locks [14] along **AD**, **BD**, and **CD** have formed, and they block further dislocation glide. Due to the high stress, a second cross-slip step may be possible on a plane parallel to

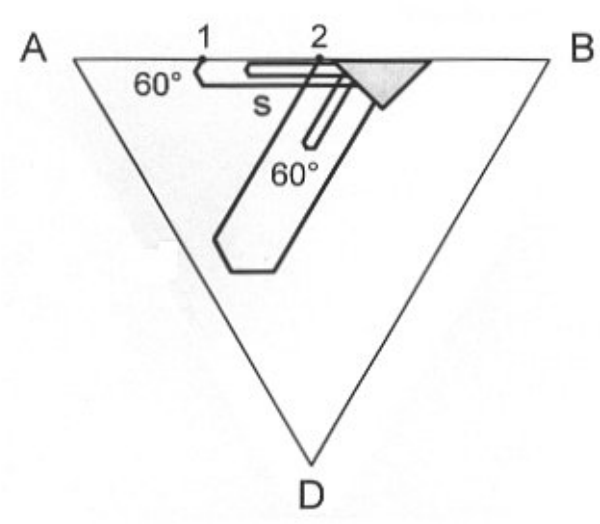

Figure 2. Scheme of the formation of hexagonal dislocation loops at a Vickers indentation. Corresponding to the nature of the {111} plane ABD, the 60° dislocations are α or β. The loops with the Burgers vector **BA** belong to the rosette slip systems, dislocations with **b** = **BD** belong to the tetrahedral slip systems. The loops consist of two screw parts of opposite sense and two 60° segments. The emergence points of dislocations at the surface (corresponding to dot-like contrasts in CL images) are 60° dislocations for the rosette slip systems (1) and screws for the tetrahedral slip system.

ABD.

In the case of the EAT, a screw with **b** = **HF** on the EFH plane cross-slips on EFH (Fig. 3b). Further cross-slip steps are less probable, since the stress on the EAT is lower [14]. A slip line may be formed as a result of the upward motion of 60° segments, as indicated in Figure 3c. Since the forward motion of the loops is supposed to be ruled by α dislocations (Figs. 2 and 3c), the backward motion is ruled by β dislocations. The regions which can be reached by cross-slip are marked gray in Figure 3. For the IAT, three displaced triangles result, as shown in Figure 1a (Cd surface). The cross-slip events on the EAT lead to a more or less triangular pattern, which appears on the Te surface (Fig. 1b).

In the following, the rosette glide will be described. A scheme of the glide planes activated for the rosette glide is shown in Figure 4. Each branch of the rosette consists of two parallel {111} planes, one of the Te type, another of the Cd type, e.g., slip occurs on the $(11\bar{1})$Te and the $(\bar{1}\bar{1}1)$Cd planes in the $[1\bar{1}0]$ direction.

The rosette glide is characterized by the movement of α and β dislocations parallel to the surface. The dragging of screw dislocations leads to the formation of hexagonal loops.

Figure 3 (*on facing page*). Cross-slips of screw dislocations on the internal apex tetrahedron for the (111)Cd surface (**a**) and the external apex tetrahedron for $(\bar{1}\bar{1}\bar{1})$Te (**b**). In the two cases, the regions that can be reached by cross slip are marked in gray. The screw dislocations are represented by their emergence points on the surface (black dots 1, 2 and 3). (**a**) Projection of the internal apex tetrahedron ABCD onto the (111)Cd surface. The screw l with the Burgers vector **b** = **AD** on the ACD plane cross-slips on a plane parallel to ABD (1 → 2). A second cross-slip step (2 → 3) occurs on a plane parallel to ACD. The slip lines sl_1 and sl_2 emerge by the movement of β dislocations towards the surface. (**b**) Projection of the external apex tetrahedron EFGH onto the $(\bar{1}\bar{1}\bar{1})$Te surface. The screw l with the Burgers vector **b** = **HF** on the EFH plane cross-slips on a plane parallel to FGH (1 → 2). The slip line sl is formed because of the upward motion of the β segment of the dislocation loop. (**c**) Cross-section of the cross-slip xs of the screw s shown in (b).

In Figure 2, the loops with the Burgers vector **b** = **BA** are examples of rosette glide. Since slip occurs on parallel Te and Cd planes, the occurrence of both α and β dislocations within one branch is supposed. This is supported by two experimental facts: first, the extension of one part of a branch is in most cases shorter, and secondly, the room temperature CL contrast of the shorter part differs from the longer one. One part shows dot-like contrast features, corresponding to individual dislocations. In the other part, the contrast of dislocations is superimposed by a diffuse background contrast. The conclusion may be drawn that this behavior is due to point defects and their interaction with α and β dislocations. Later in this chapter, the interaction between dislocations and point defects will be discussed in more detail. Considering the polarity of the 60° dislocations, it has to be concluded that α dislocations lie on planes with an obtuse angle to the (111)Cd surface. β dislocations glide on planes with an acute angle to the surface (Fig. 4). Such a conclusion takes into consideration that the extra half planes must be outside the respective tetrahedra for the rosette glide. This is equivalent to the assumption of Braun *et al*. [3] that material must be pushed away from the indenter within the prisms of the rosette glide formed by the {111} slip planes.

Neither in the part of the branch with α dislocations, nor in the part with β dislocations, CL line contrasts, which could be ascribed to screw dislocations lying parallel to the surface, are clearly visible. Two possibilities may be discussed. On the one hand, the velocity of screw dislocations may be high enough that one screw segment of the hexagonal loop (Fig. 2) has reached the surface, and the other screw has moved into a depth which is higher than the maximum information

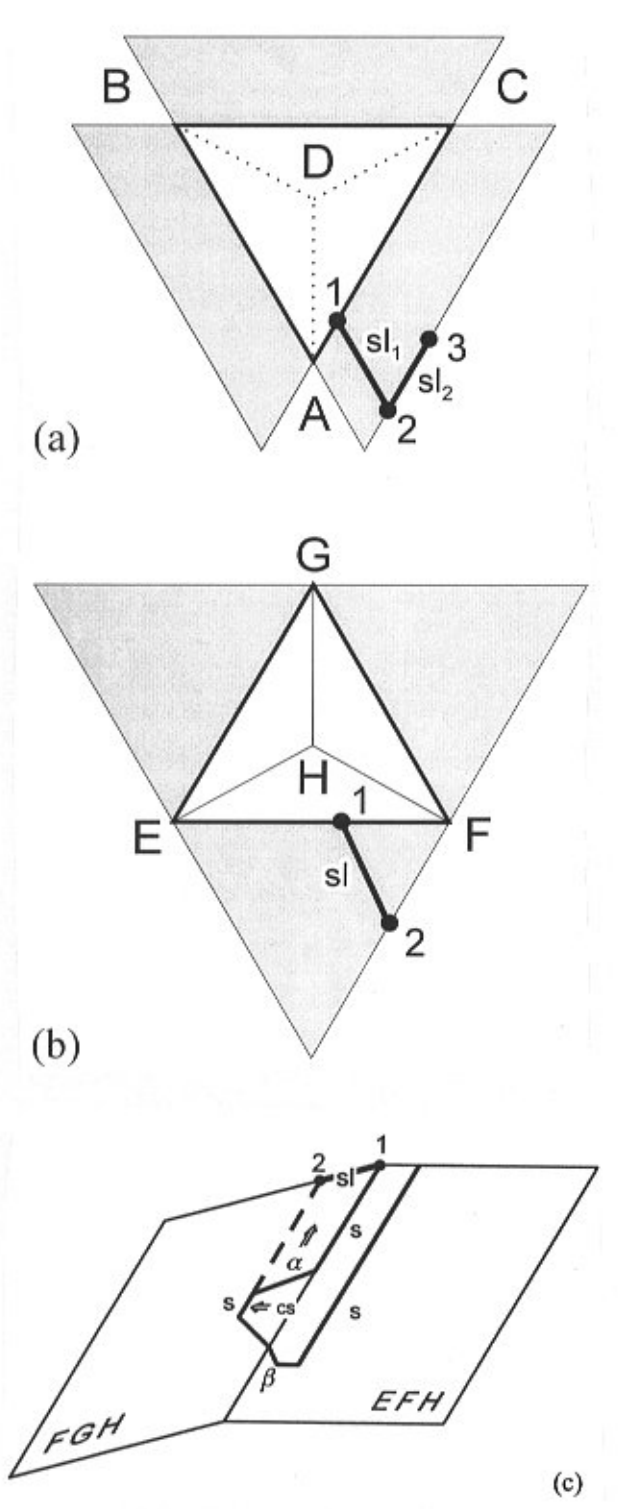

depth of the CL signal (about 5 μm in the experimental setup used here [13]). On the other hand, the CL contrast of screws or dislocations running parallel to the surface may be too

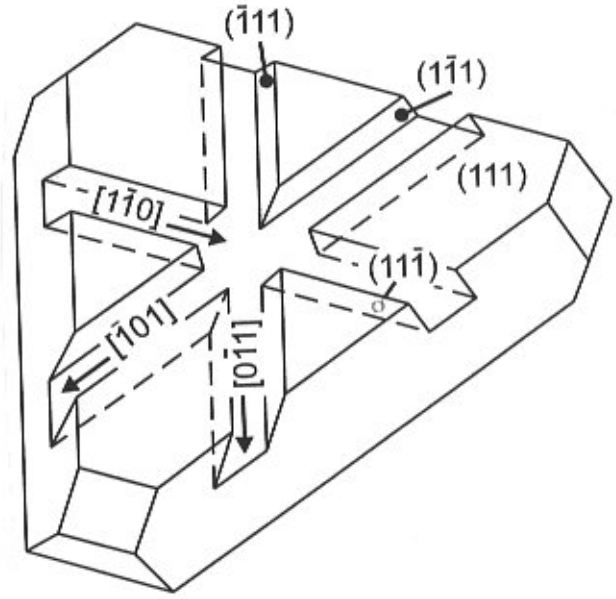

Figure 4. Slip systems of the rosette glide for a (111)Cd surface. α dislocations glide on $(1\bar{1}\bar{1})$, $(\bar{1}1\bar{1})$, or $(\bar{1}\bar{1}1)$ planes with an obtuse angle to the sample surface, and β dislocations glide on $(\bar{1}11)$, $(1\bar{1}1)$ or $(11\bar{1})$ planes with an acute angle to (111).

weak to be detectable. This case cannot be excluded, since the contrast of surface-parallel dislocations depends on several parameters - e.g., depth, recombination strength of the defect, excitation conditions.

Indentations on (110) and (001) Surfaces of CdTe

A typical example of the dislocation distribution around Vickers indentations on a (110) cleavage plane is shown in Figure 5a. A scheme of systems of rosette and tetrahedral glide analogous to that of ±(111) sample orientations can be applied to the (110) surface orientation (Figs. 5b and 5c). The tetrahedral glide proceeds by the motion of dislocation loops along the $[0\bar{1}1]$, $[\bar{1}01]$, $[0\bar{1}\bar{1}]$, and [101] directions. The arrows in Figure 5c represent the glide directions of the 60° segments of the hexagonal loops. Screw dislocations are dragged behind and cause the dot contrasts in the slip pattern near the indentation. Screw dislocations intersect the (110) surface along the $\pm[1\bar{1}2]$ or $\pm[\bar{1}12]$ directions.

As in the case of ±(111) surfaces, the cross-slip of screws may considerably influence the slip pattern of tetrahedral glide. The spread of the slip pattern in $\pm[1\bar{1}0]$ is a result of the cross-slip of screws. Screw dislocations aligned on {111} planes perpendicular to the surface may cross-slip

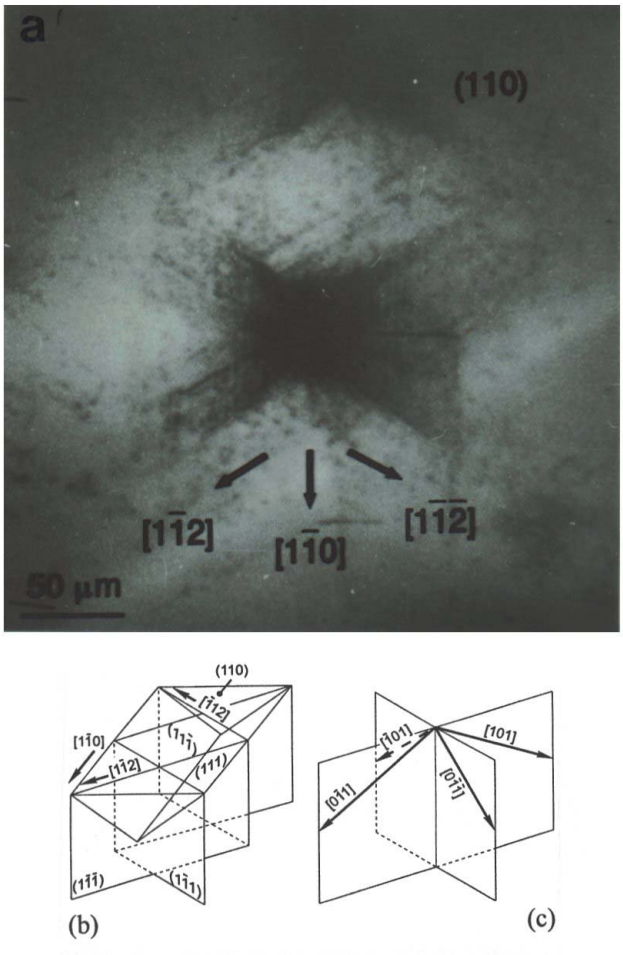

Figure 5. (**a**) CL image (sample temperature 300K, 20 kV electron beam) of the dislocation pattern around a Vickers indentation on CdTe with a (110) surface orientation. Indentation load 0.1 N. (**b**) Set of slip planes at a Vickers indentation on (110) CdTe. The (11$\bar{1}$) and (111) planes belong to the rosette glide systems, comprising the movement of dislocations loops parallel to the surface. (**c**) Slip systems of the tetrahedral glide. The arrows represent the glide directions of the 60° segments of the hexagonal loops. Screw dislocations are dragged behind and determine the extension of the slip pattern of the tetragonal glide systems as observed at the surface.

along (11$\bar{1}$) and (111) cross-slip planes. Slip lines may be formed in ±[1$\bar{1}$0] as a result of the back motion of 60° dislocations. Screw dislocations aligned on the inclined (11$\bar{1}$) and (111) planes may cross-slip along planes perpendicular to (110). This leads to the emergence of slip lines along ±[1$\bar{1}$2] and ±[$\bar{1}$12] directions.

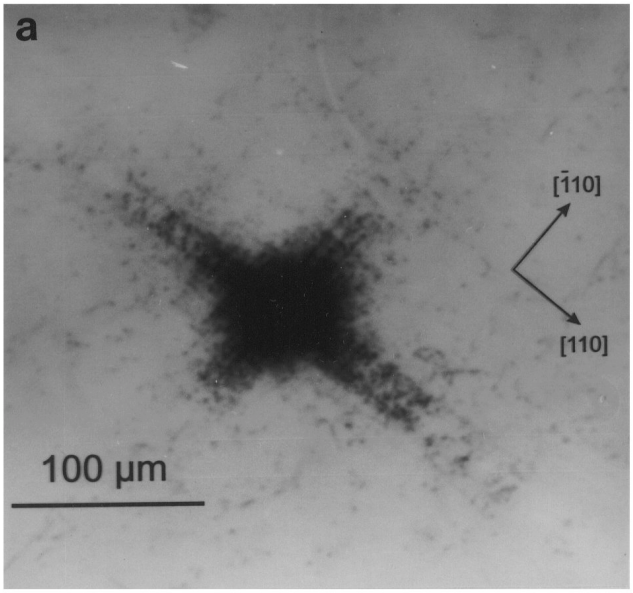

Figure 6. (**a**) Dislocation distribution near an indentation on (001) CdTe. CL image at 300 K with a 15 kV electron beam. (**b**) Rosette glide systems at an indentation on a (001) surface. In the ±[110] direction, α dislocations are gliding on (1$\bar{1}\bar{1}$) or ($\bar{1}$1$\bar{1}$). Similarly, β dislocations are moving in the ±[1$\bar{1}$0] direction on ($\bar{1}\bar{1}\bar{1}$) and (11$\bar{1}$). As a consequence of the motion of α and β dislocations, screw dislocations are expanded along ±[110] and ±[1$\bar{1}$0].

The rosette glide is characterized by a prism being formed by the (11$\bar{1}$)Te and (111)Cd planes and aligned in ±[1$\bar{1}$0] direction. The fact that the (11$\bar{1}$) and the (111) planes are of different polarity is connected with the parallel glide motion of α and β dislocations in ±[1$\bar{1}$0].

The dislocation pattern in Figure 5a is characterized by dot-like contrasts and weak lines in ±[1$\bar{1}$0], ±[1$\bar{1}$2], and ±[$\bar{1}$12]. Generally, the dots in ±[1$\bar{1}$2] and ±[$\bar{1}$12] are chains of screws, emerging at the surface as a result of their glide or cross-slip. The hardly visible dislocation lines in Figure 5a are mostly α or β dislocations formed during the cross-slip of screws. Slip lines are formed by the motion of these dislocations towards the surface.

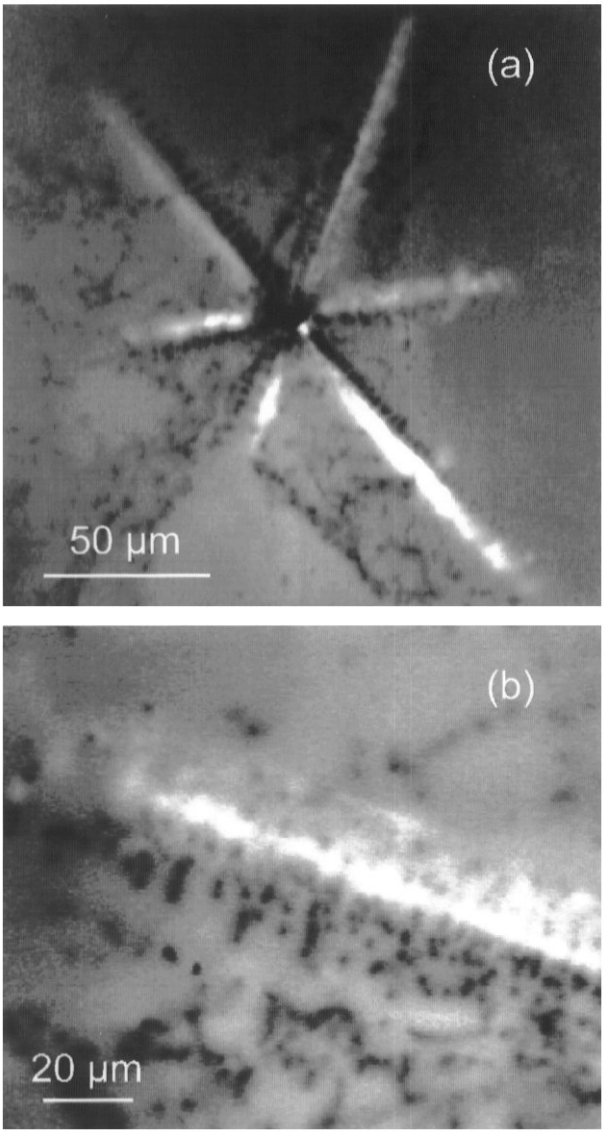

Figure 7. CL image of a dislocation rosette in (111)Cd-oriented CdTe. Sample temperature is 72K; the electron beam is 20 kV. (**a**) Whole slip pattern; (**b**) details of the [$\bar{1}$10] arm of the rosette (not the same indentations as in Fig. 7a).

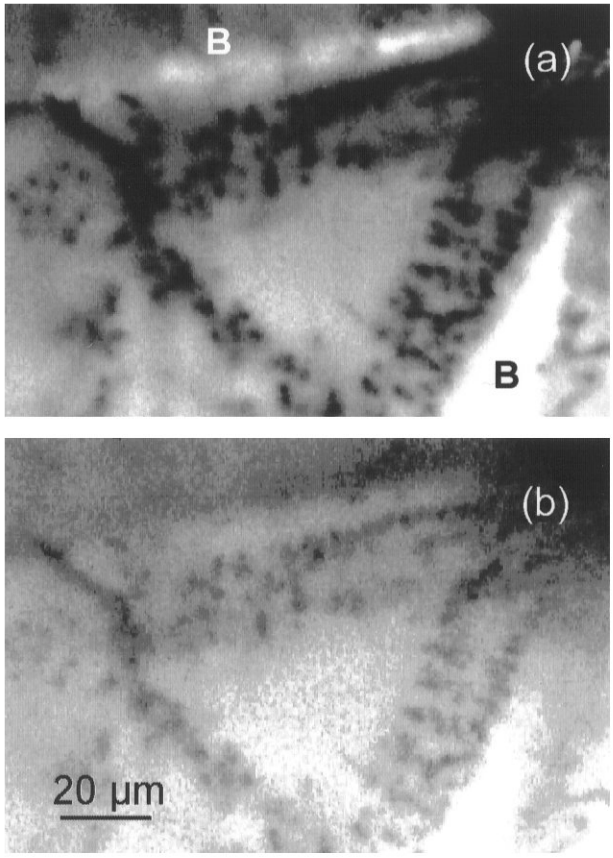

Figure 8. The same part of a dislocation rosette taken at two different temperatures. The bright regions B at 72K (**a**) are vanishing at 120K (**b**). (111)Cd-oriented CdTe, with a 20 kV electron beam.

The general model of dislocation formation as has been extensively studied for (001)-oriented III-V compounds [15, 18, 19, 26] can be adopted for cadmium telluride. A pronounced rosette glide in ±[110] and ±[1$\bar{1}$0] is found around indentations on the (001) surface of CdTe (Fig. 6a). Independent of the indentation conditions, the ±[110] branches are longer than the ±[1$\bar{1}$0] ones in most cases. They both belong to the rosette glide systems of dislocation motion parallel to the surface, which is schematically drawn in Figure 6b. A simple geometrical consideration of the position of the extra half planes of the 60° dislocations formed {e.g., the (111) plane for dislocations gliding in [$\bar{1}\bar{1}$0] on (1$\bar{1}\bar{1}$) or ($\bar{1}$1$\bar{1}$); see Fig. 6b} leads to the conclusion that α dislocations are moving in the ±[110] direction and β in the ±[1$\bar{1}$0] direction. By the motion of these 60° dislocations, screws are expanded.

Similarly to GaAs [19], glide near the indentation occurs preferentially with Burgers vectors inclined to the surface for higher loads. As for indentations on ±(111) and (110) surfaces of CdTe, cross-slip of screw dislocations is also an important feature of dislocation motion at indentations on (001). A rectangular pattern of dislocation lines is seen near the indentation site (Fig. 6a). The dot contrasts are mainly caused by screw dislocations of the tetrahedral slip systems in this region, whereas in the outermost parts of the rosette, the dots are due to 60° dislocations. The cross-slip is promoted by the fact that further dislocation glide is blocked by the formation

of Lomer-Cottrell locks along the converging {111} planes of the tetrahedral slip systems. Such locks usually determine the hardness in materials with a much lower cross-slip activity.

Relation Between Luminescence Properties of Dislocations and Generation of Point Defects

Figure 7 shows the occurrence of a local emission at temperatures below 100 K in the region of the dislocation rosette of an indentation on (111)Cd CdTe. It is visible that the bright luminescence is restricted to certain parts of the rosette. A strong degradation of the emission was observed at temperatures higher than 100 K (Fig. 8). No bright contrasts were found during room temperature observations (Figs. 1, 5 and 6). The bright features are occurring for ±(111) surfaces in that part of the rosette where according to the slip model (Fig. 4), the faster α dislocations are moving. A similar emission was found near indentations on (110) and (001) surfaces. However, in the case of indentations on (001), it is not restricted to the ±[110] rosette arms with α dislocations, but also found in the ±[1$\bar{1}$0] β arms. The bright contrast is screened by the strong non-radiative recombination due to the high dislocation density near the indentation in the region of tetrahedral glide.

Cathodoluminescence spectra were measured in the dislocation rosette and in the undeformed crystal (Fig. 9). Only the peak at about 1.60 eV, which has been related to donor-bound excitons D^0-EX [5], was found in the matrix. A new peak at 1.48 eV (named DL) is found in the region of the bright contrasts of the rosette. The intensity of the D^0-EX line strongly decreases in the dislocation rosette in relation to the DL line at 1.48 eV.

The DL line disappeared after annealing at 500 K for 10 minutes, and the rosette pattern showed no difference at room and liquid nitrogen temperature.

The DL emission seems to be closely related to dislocations (dot-like bright contrasts in Fig. 7b). Two possible models may be discussed for defects responsible for the DL line. The strong DL emission could be attributed to localized defects on the dislocation line or dislocation core states. Such defects may be jogs, constrictions due to the cross-slip discussed above, or vacancies in the dislocation core. A similar model has been proposed recently by Sekiguchi and Sumino [23] in order to explain the dislocation-related luminescence in silicon. It was proposed, after deformation experiments in very clean conditions, that the D1 and D2 photoluminescence lines in Si are related to dislocation-reaction products, like jogs [23].

A dislocation core-state model of the DL emission in CdTe is not able to explain the different distributions of the bright regions for ±(111) and (001) surfaces. From the distribution on ±(111) surfaces, a relation to one dislocation type (α or β) would be expected. However, this interpretation is not in agreement with the pattern on (001), where both the ±[110] and ±[1$\bar{1}$0] arms are bright at lower temperatures.

In order to investigate the nature of point defects in the deformed region of indentations, spectroscopic defect-level investigations were performed by the Göttingen group [9, 11, 16, 29]. Levels of 0.73 eV below the conduction band, or 0.35 and 0.45 eV above the valence band, were detected in DLTS experiments. An attempt has been made to correlate the electronic states to dislocations. The conclusion has been drawn that the longer branch of the dislocation rosette show a higher electrical activity [16]. The trap concentration correlated with the dislocation density, but was at least one order of magnitude higher than the possible number of core states [11]. Therefore, it was concluded that the signal is probably not an intrinsic property of the dislocation core, but due to a point defect cloud. The defect level of 0.73 eV was attributed to intrinsic point defects. The concentration of these defects was found to be at a factor of three higher for the faster dislocations [16].

It is concluded that the generation of native point defects in the course of the dislocation motion is responsible for the occurrence of the bright DL regions. The 1.48 eV line found here in the dislocation rosette was attributed to products of plastic deformation [2] and has been recently assigned to Cd-vacancy-related defects [1, 7]. Díaz-Guerra *et al*. (1995) [7] also studied CL near micro-indentations. Though they could not resolve the strong correlation of the 1.48 eV luminescence to the vicinity of dislocations, a similar bright luminescence was found and attributed to vacancies.

The vacancies are thought to be generated by the interaction of dislocations belonging to the rosette glide systems with dislocations of the tetrahedral glide systems. The intersection of such dislocations leads to the formation of jogs on screw and 60° dislocations. Part of these jogs is not glissile and is dragged behind the gliding dislocations. The vacancies generated by jog dragging are not mobile enough in the room-temperature indentation experiment and remain located near the dislocations. The asymmetry of the rosette on ±(111) CdTe, i.e., the existence of a bright rosette part with the faster dislocations and a dark part with the slower dislocations, can be understood in such a way that the interaction of dislocations in the tetrahedral and rosette glide systems is not symmetrical. On one side of the rosette arm, the interaction occurs between α and α dislocations, on the other side between β (rosette glide system) and α dislocations (tetrahedral glide). The intersection of dislocations of the same type is much more frequent and leads to jog dragging in one part of the rosette arm. The vacancies related to the DL luminescence are found for indentations on (001) in both the ±[110] and ±[1$\bar{1}$0] because there the effective cutting of dislocations with the same type occurs in both arms.

It should be noted that differences in the DLTS signal

of α and β dislocations generated at indentations on (001) InP have been reported [30]. In that case, the differences have been explained by the occurrence of impurity clouds. It cannot be excluded that the vacancies generated by jog dragging in CdTe are bound to impurities and produce in such a way the 1.48 eV line.

Conclusions

The cathodoluminescence scanning electron microscopy is a suitable tool to study the defect configuration after local plastic deformation of cadmium telluride at room temperature. The slip systems occurring at micro-indentations in CdTe can be divided into those with a Burgers vector **b** parallel to the surface (rosette slip systems) and those with **b** inclined (tetrahedral slip systems). The first ones result in the case of the ±(111) and (001) surfaces to dislocation rosette patterns extended over some 100 μm. The rosette slip systems are less important for a (110) surface.

CdTe is much more ductile than silicon or gallium arsenide, leading to a lower number of cracks after indentation. The higher glide mobility is connected with the larger extension of dislocation rosette. The tetrahedral slip systems determine the arrangement of dislocations underneath the Vickers indentation. Since a multitude of $<1\bar{1}0>\{111\}$ systems are activated, a high density of dislocations with different Burgers vectors is formed.

The hardness is mainly determined by tetrahedral glide on converging planes, leading to the formation of locks for dislocation glide. In CdTe, the locks are frequently bypassed by the cross-slip of screws. The low hardness of CdTe may therefore be connected with a high cross-slip activity observed in this study in all micro-deformation experiments.

The cathodoluminescence studies testify the production of point defects by moving dislocations. The bright luminescence features found in CL images at temperatures below 100 K are caused by the 1.48 eV line. The thermal stability of the defects is low. The centers detected here are not related to dislocation core states, which is in agreement with former DLTS measurements.

The point defects near dislocations are probably vacancies, which are generated by a jog dragging mechanism. A hexagonal structure of dislocation loops is supposed with 60° front segments, followed by screws. The interaction of such loops belonging to different slip systems provides the necessary number of jogs. The generated vacancies may influence the dissociation behavior of dislocation. The low stacking fault energy of CdTe is not only connected with the high cross-slip activity but should also result in a high number of stacking faults near indentation as in GaAs [15, 18, 19]. The point defect cloud, however, impedes the leading partial dislocations in such a way that the formation of stacking fault ribbons or microtwins, as in the case of GaAs, is blocked. Consequently, intrinsic stacking faults were rarely observed near indentations, in transmission electron micrographs.

References

[1] Allen JW (1995) Spectroscopy of lattice defects in tetrahedral II-VI compounds. Semicond Sci Technol **10**: 1049-1064.

[2] Babentsov VN, Gorban' SI, Sal'kov EA, Tarbaev NI (1987) Low-temperature photoluminescence of cadmium telluride single crystals containing structure defects. Sov Phys Semicond **21**: 1043-1045.

[3] Braun C, Helberg HW, George A (1986) Surface damage of CdTe produced during sample preparation, and determination of dislocation types near micro-hardness indentations. Phil Mag A **53**: 277-284.

[4] Bredikhin SI, Shmurak SZ (1983) Deformation luminescence in II-VI crystals. J Physique **44**: C4/183-C4/188.

[5] Brink DJ, Kunert HW (1995) Photoluminescence of CdTe thin films containing a mixed crystal orientation. J Appl Phys **78**: 6720-6725.

[6] Brown PD, Durose K, Russel GJ, Woods J (1990) The absolute determination of CdTe crystal polarity. J Cryst Growth **101**: 211-215.

[7] Díaz-Guerra C, Pal U, Fernández P, Piqueras J (1995) Deep level cathodoluminescence in deformed CdTe crystals. Phys Stat Sol A **147**: 75-80.

[8] Escaig B (1968) Sur le glissement dévié des dislocations dans la structure cubique a faces centrées (About the deviation of dislocation glide in the face-centered cubic structure). J Physique **29**: 225-239.

[9] Gelsdorf F, Schröter W (1984) DLTS study of the influence of plastic deformation on deep levels in n-type CdTe. Phil Mag A **49**: L35-L42.

[10] Gottschalk H, Patzer G, Alexander H (1978) Stacking fault energy and ionicity of cubic III-V compounds. Phys Stat Sol A **45**: 207-217.

[11] Haasen P, Müller H, Zoth G (1983) The plasticity of a semiconducting compound: CdTe, electrical measurement and chemomechanical effect. J Physique **44**: C4/365-373.

[12] Hall EL, Vander Sande JB (1978) Plastic deformation behavior and dislocation structure of CdTe single crystals. J Am Ceram Soc **61**: 417-425.

[13] Hergert W, Hildebrandt S, Pasemann L (1987) Theoretical investigations of combined EBIC, LBIC, CL and PL experiments. Phys Stat Sol A **102**, 819-828.

[14] Hirsch PB, Pirouz P, Roberts SG, Warren PW (1985) Indentation plasticity and polarity of hardness on {111} faces of GaAs. Phil Mag B**52**: 759-784.

[15] Höche H-R, Schreiber J (1984) Anisotropic deformation behaviour of GaAs. Phys Stat Sol A **86**: 229-236.

[16] Hümmelgen I (1993) Deep levels associated with α and β dislocations in n-CdTe. J Mater Sci Lett **12**: 451-452.

[17] Iwanaga H, Tomizuka A, Shibata N, Mochezuki M (1986) Etch pits and polarity identification in CdTe, HgSe and HgTe crystals. J Cryst Growth **74**: 113-117.

[18] Lefebvre A, Androussi Y, Vanderschaeve G (1987) A TEM investigation of dislocation rosettes around vickers indentations in GaAs. Phys Stat Sol A **99**: 405-412.

[19] Leipner HS, Schreiber J, Surowiec M (1989) Perfect and partial dislocations in microdeformed GaAs. In: Electron Microscopy in Plasticity and Fracture Research of Materials. Messerschmidt U, Appel F, Heydenreich J, Schmidt V (eds.). Akademie-Verlag Berlin, Germany. pp. 193-198.

[20] Lu G, Cockayne DGH (1983) Dislocation structures and motion in II-VI semiconductors. Physica B **116**: 646-649.

[21] Osip'yan YuA, Petrenko VF, Zaretskiî AV, Whiteworth RW (1986) Properties of II-VI semiconductors associated with moving dislocations. Adv Phys **35**: 115-188.

[22] Riviére A, Sieber B, Riviére JP (1991) Cathodoluminescence imaging of microindented {111} CdTe. Microsc Microanal Microstruct **2**: 503-514.

[23] Sekiguchi T, Sumino K (1995) Cathodoluminescence study on dislocation-related luminescence in silicon. Mater Sci Forum **196-201**: 1201-1206.

[24] Sieber B, Philbert J (1987) EBIC contrast of defects in CdTe. Phil Mag B **55**: 575-598.

[25] Sumino K, Shimizu H (1975) Polarity in bending deformation in InSb crystals. II. Theory and supplementary experiments. Phil Mag **32**: 143-157.

[26] Surowiec MR, Tanner BK (1987) X-ray topographic study of dislocations around indents on {111} surfaces of indium antimonide. J Appl Cryst **20**: 499-504.

[27] Takeuchi S, Suzuki K, Maeda K (1984) Stacking-fault energy of II-VI compounds. Phil Mag A **50**: 171-178.

[28] Tarbaev NI, Schreiber J, Shepelskii GA (1988) Physical properties of $A^{II}B^{VI}$ semiconductor crystals after plastic deformation at low temperature. Phys Stat Sol A **110**: 97-106.

[29] Zoth G, Schröter W (1988) Observation of a multiply charged defect in p-type CdTe. Phil Mag B **58**: 623-633.

[30] Zozime A, Schröter W (1990) Deep levels associated with α and β dislocations in n-type InP. Appl Phys Lett **57**: 1326-1327.

Discussion with Reviewers

Z. Radzimski: What was the purity of the investigated material and the experimental environment?

Authors: We used unintentionally doped *p*-type material with a low compensation level, as reported elsewhere by other authors, who used the same CdTe sample material [32]. Residual impurities are Cu and Li. Grown-in dislocations exhibit impurity clouds resulting in CL halo contrasts, but no such halos appear for fresh dislocations introduced by micro-indentation. As we investigated fresh glide dislocation immediately after the indentation experiment at room temperature (on air), the influence of impurities on the luminescence behavior in the deformed area may be minor. A further indication is that the luminescence behavior observed near the micro-indentations has a long-term stability.

G.A. Shepelskii and N.I. Tarbaev: As for the defect type identification, the uncertainty still remains. In particular, the possibility that interstitials are involved can not be excluded.

Authors: We are quite sure that the generation of different types of point defects is very probable in the micro-indentation experiment. Especially the formation of interstitials in the course of jog dragging can not be excluded. Our luminescence spectra show a characteristic band at 1.48 eV (DL). The nature of luminescence bands around 1.48 eV has been the subject of several papers [33, 35, 39]. Obviously, different defects may give rise to the luminescence in this region. The most probable candidate for the DL band is the A center. As for the structure of this complex, a cation vacancy, which may be bound to a shallow donor, has been considered most likely [35].

We have evidence from positron lifetime spectroscopy for the generation of Cd vacancies during plastic deformation. The positron technique is sensitive to vacancy-like defects, if they are neutral or negatively charged. Vacancies in the anion sublattice of II-VI compounds cannot be detected by positrons, since they are positively charged [36]. We detected a higher positron lifetime after deforming the CdTe crystal by a high number of micro-indentations. The increase of the positron lifetime has been attributed to the generation of cadmium vacancies. The thermal annealing of the Cd-vacancy-induced positron lifetime was observed around 500 K. Simultaneously, the luminescence band at 1.48 eV vanished after the same heat treatment. This may be an indication that the same defect reaction was observed both by the change of the cathodoluminescence and positron annihilation signals. Furthermore, the vacancy signal of the positron lifetime measurements can be quenched by Ag diffusion at room temperature [37], since the reaction $V_{Cd} + Ag_I \rightarrow Ag_{Cd}$ occurs. The bright contrasts in the CL images disappeared after the diffusion experiment.

G.A. Shepelskii and N.I. Tarbaev: Using the results of the Göttingen group as an argument for the authors model is doubtful because the energetic states found there are too deep to be responsible for states involved in the DL band at 1.48 eV.

Authors: As was stated above, other point defects, e.g., interstitials, or defects bound to the dislocation core are generated during micro-indentation. We take the results of the Göttingen group as a support for the point-defect hypothesis. Anyway, it is likely that different point-defect species are responsible for DLTS lines and for the

cathodoluminescence peak, respectively. It should be noted that information about interstitials, generated as well by dislocation intersection, is scarce.

In the current state of the investigations, we cannot exclude other models in addition to the interpretation given above. Now, the model of Cd vacancies localized near α dislocations is preferred. Interestingly, Seto *et al*. attributed, in a recent paper, the 1.48 eV luminescence to defect complexes in the strain field of dislocations [40]. Additional experiments are necessary to study the properties of the DL luminescence line, such as the phonon structure and the temperature dependence, in detail. Alternative models have to be discussed, e.g., the Y_0 luminescence, which is a deep state related to an exciton bound to the dislocation line [34].

T. Sekiguchi: Is there some relation among the velocities of different types of dislocations, for example, are β dislocations faster than α or screws?

Authors: No quantitative measurements of the dislocation velocity are known for cadmium telluride. The rosette branches in ±[110] directions are longer than the ±[1$\bar{1}$0] arms for indentations on the (001) surface of the CdTe crystals under investigation. This immediately implies that 60° α dislocations are faster than β. The slip patterns around indentations on the (110) surface can be explained by assuming that the mobility of screw dislocations is close to the mobility of β dislocations. However, it is hard to draw quantitative results from indentation experiments, since the non-homogeneous stress field influences the length of the rosette arms. Furthermore, recovery processes have to be taken into account.

The conclusion on the mobility ratio drawn above is based on the formation of hexagonal dislocation loops, as sketched in Figure 2. It should be mentioned that a strong dependence of the dislocation velocity on doping as observed in GaAs [38] may also occur in CdTe, i.e., for other doping conditions, the velocity ratio may change and, for instance, β may become faster than α dislocations.

T. Sekiguchi: It is interesting that the different combinations of interacting dislocations are the cause of different luminescence features. However, is the interaction between α dislocations able to create Cd vacancies? The jogs created by the cutting between α dislocations may have a character like β or screw dislocations.

Authors: The formation or motion of an elementary jog with a height of one lattice distance requires in a compound semiconductor that atoms of both sublattices are either emitted or absorbed. For instance, in CdTe, in dependence on the sense of the jog, vacancies (both V_{Cd} and V_{Te}) or interstitials (both I_{Cd} and I_{Te}) are emitted by the non-conservative motion of the dislocation. Otherwise, the dislocation line would jump with the jog from the glide-set to the shuffle-set position, which is regarded for dissociated dislocations in the sphalerite structure as energetically unfavorable. For elementary jogs, it gives no sense to attribute them a character like β or screws, because the atomic arrangements may be very different for long and straight dislocation segments.

It is possible to calculate the number of point defects emitted by the intersection of dislocations. The number of point defects formed per unit length was given by Amelinckx [31] as

$$N = \frac{1}{\Omega} \frac{e_1 \cdot u \times e_2}{| e_1 \cdot u \times e_2 |} b_1 \cdot u \times b_2 \qquad (2)$$

(Ω = atomic volume, **u** = direction of motion of the dislocation with the Burgers vector $\mathbf{b}_1$ and the line vector $\mathbf{e}_1$. $\mathbf{b}_2$ and $\mathbf{e}_2$ are the Burgers vector and the line vector of the static dislocation, respectively.) The first term determines the sign, i.e., whether interstitials or vacancies are formed, the second one gives the number of point defects (volume defined by $\mathbf{b}_1 \cdot \mathbf{u} \times \mathbf{b}_2$).

Additional References

[31] Amelinckx S (1979) Dislocations in particular structures. In: Dislocations in Solids. Nabarro FRN (ed.). North-Holland, Amsterdam, The Netherlands. pp. 67-460.

[32] Becker U, Zimmermann H, Rudolph P, Boyn R (1989) Optical study of the impurity distribution in vertical-Bridgman-grown CdTe crystals. Phys Stat Sol A **112**: 569-578.

[33] Chamonal JP, Molva E, Pautrat JL (1982) Identification of Cu and Ag acceptors in CdTe. Sol State Commun **43**: 801-805.

[34] Dean PJ, Williams GM, Blackmore G (1984) Novel type of optical transition observed in MBE grown CdTe. J Phys D **17**: 2291-2300.

[35] Hofmann DM, Meyer BK, Probst U, Benz KW (1990) Optical and optically detected magnetic resonance investigations on the A-center complex in CdTe. J Cryst Growth **101**: 536-539.

[36] Krause R, Neubert M, Drost T, Hörstel W, Polity A, Kiessling FM, Paitz U, Zlomanov V, Mäkinen S (1992) Vacancies in II-VI and IV-VI compound semiconductors studied by positron lifetime spectroscopy. Mater Sci Forum **105-110**: 333-340.

[37] Krause-Rehberg R, Zimmermann H, Klimakow A, Drost T (1992) Occupation of the Cd vacancy site in CdTe by diffusing silver atoms observed by positron annihilation. Phys Stat Sol A **134**: K45-K47.

[38] Maeda K (1985) A unified view on the Peierls mechanism in covalent crystals. In: Dislocations in Solids. Suzuki H, Ninomiya T, Takeuchi S (eds). University of Tokyo, Japan. pp. 425-428.

[39] Norris CB, Barnes CE (1977) Cathodoluminescence studies of the 1.4 eV bands in CdTe. Rev Phys Appl **12**: 219-

227.

[40] Seto S, Tanaka A, Takeda F, Matsuura K (1994) Defectinduced emission band in CdTe. J Cryst Growth **138**: 346-351.